Thu Dau Mot University Journal of Science
ISSN 2615 - 9635
journal homepage: ejs.tdmu.edu.vn

Benchmarking study between Lagamine and Comsol Solvers for Finite Element Thermal Analyses of Directed Energy Deposition Process

by ***Bui Sy Vuong, Tran Van Xuan*** *(Thu Dau Mot University),*
Le Van Thao *(Advanced Technology Center, Le Quy Don Technical University, Hanoi)*

Article Info: *Received Sep. 14th, 2023, Accepted Oct. 11th, 2023, Available online Dec.15th, 2023*

Corresponding author: xuantv@tdmu.edu.vn

https://doi.org/10.37550/tdmu.EJS/2023.04.502

ABSTRACT

This work presents a benchmarking study between Lagamine, an in-house developed finite element (FE) code, and COMSOL Multiphysics® (Comsol) commercial software in thermal analyses to investigate their capability in modeling complex manufacturing processes. For this purpose, two case studies, including a NAFEMS benchmark for heat transfer with convection and a Directed Energy Deposition (DED) of a bulk sample, were used as test cases. The simulation models using Lagamine and Comsol solvers for each case were described. The underlying algorithms and theories, as well as the software development, are investigated. The computational results indicate slight differences between Lagamine and Comsol solutions in both case studies. For the NAFEMS test case, the results obtained with the Comsol solver appear to be less dependent on the mesh size than those obtained with Lagamine. For the DED test case, within the chosen configurations of Lagamine and Comsol codes, the maximum difference in the highest peak temperatures obtained from the two codes is about 20%. From an engineering point of view, it is suggested to determine the parameters of the FE model consistently with the selected FE code to provide the best match with experimental observations.

Keywords: *Directed Energy Deposition, finite element method, Lagamine, COMSOL Multiphysics®, thermal analysis*

1. Introduction

In recent decades, various additive manufacturing (AM) processes have been developed for the fabrication of complex geometry and high-quality metal parts, and for reparation (Bikas, 2016; Frazier, 2014). Among them, Direct Energy Deposition (DED) has been widely used due to its overwhelming advantages of high-building rate and controllable product properties. However, the high capital cost, for example, the increased costs of DED machines and expenditure for quality control and measurement equipment, is the principal disadvantage of DED, restricting its application in practice. Besides, during an AM process, especially that of DED, a moving energy source is used to melt metallic powders and deposit the melted materials layer-by-layer onto the workpiece. The deposited materials could be re-melted throughout the subsequent layers under the effect of the absorbed heat, causing several cyclic thermal loads on a material point during the heating and cooling processes. To reduce the number of trial-and-error experiments needed before performing real tests, numerical simulations based on the Finite Element Method (FEM) have been largely used and can be considered as an efficient tool for thermal analysis and process parameter optimization.

So far, numerous simulations have provided detailed information regarding the evolution of the temperature field occurring during DED processes. For example, Jiazhu et al. (2019) carried out a numerical-experimental study to observe the thermal behavior during the Laser Engineered Net Shaping (LENS) process. The temperature distribution within the built component was achieved via the numerical simulation, which was then validated with the experimental observations. Jardin et al., (2020) performed a sensitivity analysis based on material thermophysical properties and environmental conditions, i.e., convection and emission coefficients, for the modeling of a DED-fabricated thin wall from high-speed steel. Kiran et al., (2020) extended an FE model developed for welding simulation to analyze DED processes for large-size parts. Recently, a hybrid method coupling numerical simulated data with surrogate models developed by Machine Learning (ML) techniques to determine the optimal parameters provides attractive results (DebRoy et al., 2021; Johnson et al., 2020). This method requires huge data samples generated from numerical simulations, raising the demand for reducing costs in terms of computing, license, and human resources for data generation, leading to the need for the use of open-access software. More importantly, it is indispensable for computational software to provide reliable results in the case of modeling complex manufacturing processes. This aims to facilitate the verification of the software to assure its capabilities and improve credibility.

So far, numerical simulations for AM processes, especially for DED, were conducted using either commercial FEM software, e.g., ANSYS (Tan et al., 2020), COMSOL Multiphysics® (Nie et al., 2021), and Abaqus (Kiran et al., 2020), or open-source/in-house developed codes, e.g., Cast3M (Chergui 2021), Lagamine (Jardin et al., 2020; Tran

et al., 2017), SIERRA (Stender et al., 2018). The usefulness of the former software group is well-established in the literature. The advantage of the latter group is that it usually provides more features frequently limited or unsupported in the first group. For example, running a vast number of simulations with commercial software is costly in the sense that multi-license, which is usually expensive, is required. In contrast, the use of an open-source or in-house developed code is free. However, using the developed code requires much effort to validate its accuracy and effectiveness before applications. Besides, commercial software is often delivered as a black-box code, which is not easy to modify to simulate the phenomena arising from the ongoing research. This limit is, however, addressed by the in-house open-access software. Therefore, it is essential to benchmark the results between at least two codes from the two above-mentioned code groups, which can help better assess the suitability of the selected codes in modeling complex processes.

Lagamine is an in-house FEM code developed at the University of Liège since the 1980s to model metal forming processes (Pierry & Wang, 1994). The code has been successfully employed to simulate numerous manufacturing processes (Guzmán et al., 2021; Neira Torres et al., 2017; Pascon et al., 2006). Recently, its application has been significantly extended to various AM processes fabricating different specimen shapes, such as bulk sample (Mertens et al., 2020), thin wall (Jardin et al., 2020), notch repair (Tran et al., 2017), and for different types of metals, e.g., AlSi10Mg (Mertens et al., 2020), 316L stainless steel (Fetni et al., 2021), high-speed steel (Jardin et al., 2020; Jardin et al., 2019). In these studies, the simulation results have been reasonably well validated with experimental measurements for temperature history, melt pool depth, microstructure features, and mechanical properties. As discussed earlier, while Lagamine appears to be attractive due to its performance and capacity to provide open access to perform thousands of simulations for parametric and optimization studies, this code has not yet been widely used in the research community outside the University of Liege. This hesitation can be overcome by thoroughly conducting an objective benchmarking of this software with a commercial one. The benchmarking will not only allow analyzing Lagamine software's performance but also provide insights and recommendations for manufacturing engineering to support software selection as well as the verification and validation of the computational results.

This work aims to present a benchmarking study between the Lagamine code and the COMSOL Multiphysics® software (Comsol), one of the most commonly used commercial FE software for modeling the design and processes, in particular for thermal analysis in AM processes (Benarji et al., 2020; Courtois et al., 2014; Le et al., 2019; Scipioni Bertoli et al., 2017; Tran & Lo, 2018). Besides, it has been shown that the investigation of physical phenomena resulting from an AM process, as well as the associated mechanical and structural behaviors at different scales, is governed by thermal analysis (Ahn, 2021; Papazoglou et al., 2020). Therefore, a standard NAFEMS benchmark for thermal convection was first investigated. The simulation results of this

study, obtained using the two above-mentioned codes, are presented in Section 2. The following section details a benchmarking study in terms of algorithms and computational results for the 2D thermal simulations of a DED process, which was then used to manufacture a bulk sample. Based on the simulation results, the advantages and disadvantages of the two codes in thermal analysis for cyclic thermal loads generated in DED processes are finally discussed.

2. NAFEMS benchmark: 2D heat transfer with convection

2.1. Description of the NAFEMS benchmark test

The NAFEMS benchmark database is recommended by the National Agency for Finite Element Methods and Standards (The Standar NAFEMS Benchmarks, 1990) to determine the accuracy of an analysis code. This study adopts one of the benchmark problems, two-dimensional heat transfer with convection, to verify the performance of the Lagamine solver for thermal analyses. The challenge has been widely used to validate the performance of various FEM codes, such as Abaqus (Abaqus Analysis User's Guide, n.d), Diana FEA (DIANA FEA User's manual, n.d), Tydn (Two-dimensional thermal analysis, n.d), and FEMLAB (FEMLab validation, n.d).

In this benchmark, thermal loads are assumed to act on a two-dimensional 0.60x1.00 m2 rectangle ABCD, as shown in Fig. 1. The tested material has a thermal conductivity of 52 W/(m•°C). The top and right boundaries, corresponding to the edges DC and BC, are subjected to convection to the ambient environment. The heat transfer problem is defined by a surface convection coefficient of 750 W/(m2•°C) and an ambient temperature held at 0°C. A prescribed temperature of 100°C is applied along the edge AB and kept unchanged during heat transfer. The edge DA is thermally insulated. The target temperature at point E located on edge BC, as shown in Fig. 1, is expected to be 18.25°C (The Standard NAFEMS Benchmarks, 1990).

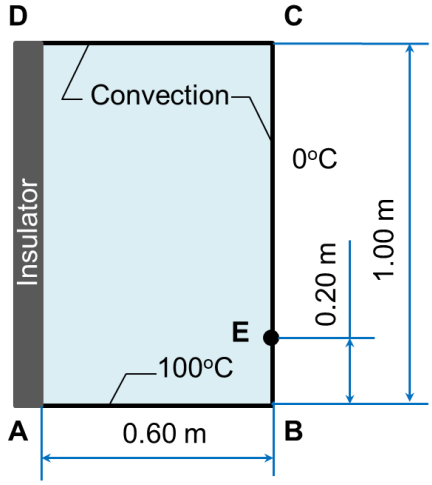

Figure 1. Description of the 2D heat transfer with convection problem.

2.2. Finite element model

To evaluate the performance of the Lagamine and Comsol solvers in terms of calculation accuracy and computing time, four meshes with different refinements were defined. In detail, regular meshes were used with the number of divisions along the AB and BC edges of 3x5, 6x10, 12x20, and 24x40, respectively. The characteristics of the meshing cases are listed in Table 1.

TABLE 1. Meshing cases and their corresponding characteristics.

Meshing case	Number of divisions along AB and BC	Number of elements	Element size (mm^2)
1	3x5	15	$4x10^4$
2	6x10	60	$1x10^4$
3	12x20	240	$2.5x10^3$
4	24x40	960	625

In the Lagamine code, the plate is modeled with linear four-node two-dimensional heat transfer elements BLZ2T (Zhu & Cescotto, 1995). BLZ2T is an assumed strain mixed thermo-mechanical finite element based on the Hu-Washizu variational principle using a unified framework with uniform reduced integration and selective numerical integration. In this application, only the thermal degrees of freedom are activated. An integration scheme based on either the first-order (IP = 1) or the second-order (IP = 4) of numerical integration is implemented. It is notable that the Lagamine code only provides a solver for time-dependent heat transfer problems. Therefore, a heat capacity of 36.0 J/(g·K) was defined, and the temperature field was reported at a target time of 10 s to reach the stationary state in these simulations.

The Comsol software provides a stationary heat transfer solver that was used to analyze the problem. The plate is modeled as a single domain and discretized by two-dimensional four-node elements QUAD with four integration points (Zhu & Cescotto, 1995). Several shape functions are available in the software, i.e., from linear to quintic orders of Lagrange and serendipity functions. The linear shape function was adopted in this application. The meshing scenarios and boundary conditions employed in the two codes are the same, which were described previously in Section 2.1.

2.3. Result comparison

Fig. 1 shows the predicted temperature at point E obtained from the Lagamine and Comsol codes for different meshes. To qualify these numerical predictions, the relative error between the reference temperature TREF = 18.25 °C at point E provided by NAFEMS and each numerical result (TFEM) is calculated as follows:

$$\delta = \frac{|T_{FEM} - T_{REF}|}{T_{REFF}} \times 100\% \quad (1)$$

The result is illustrated in Fig. 2. As can be seen in the figure, for the Lagamine code, the results obtained from a coarse mesh (meshing case 1) significantly deviate from the

reference solution with a relative error δ reaching about 60%, no matter which the number of integration points is. In the case of finer meshes, the relative errors δ are significantly diminished, remaining lower than about 3%, as illustrated in Fig. 1. The results of one integration point method (IP = 1) fluctuate slightly around the reference value with a maximum relative error δ of about 3% (see Fig. 1). By employing four integration point method (IP = 4), the predicted temperature accuracy increases with the number of elements. Regarding the Comsol solver, its results appear identical to those obtained by the Lagamine code employing four integration points, as shown in Fig. 2. With a proper mesh size (meshing case 4), both Lagamine and Comsol codes show the lowest relative error of 0.22%, which is sufficient to validate their performance in this particular benchmark.

Fig. 3 shows the temperature distribution within the plate predicted by the Lagamine code (IP = 4) and the Comsol software for meshing case 4. It can be seen that the temperature field predicted by Lagamine is in good agreement with that predicted by Comsol. In brief, both Lagamine and Comsol appear to be able to provide sufficiently accurate results for the NAFEMS benchmarking study for heat transfer with convection.

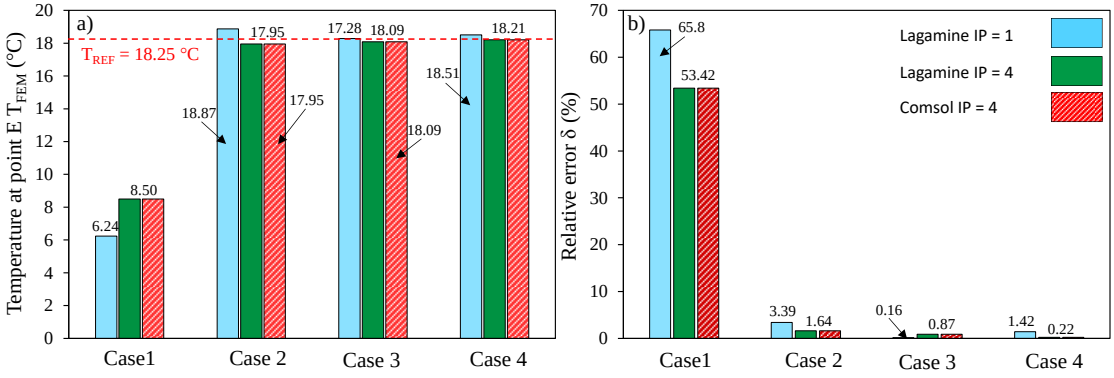

Figure 2. a) Temperature at point E predicted by the Lagamine code and Comsol solver for different meshing cases, and b) corresponding relative error.

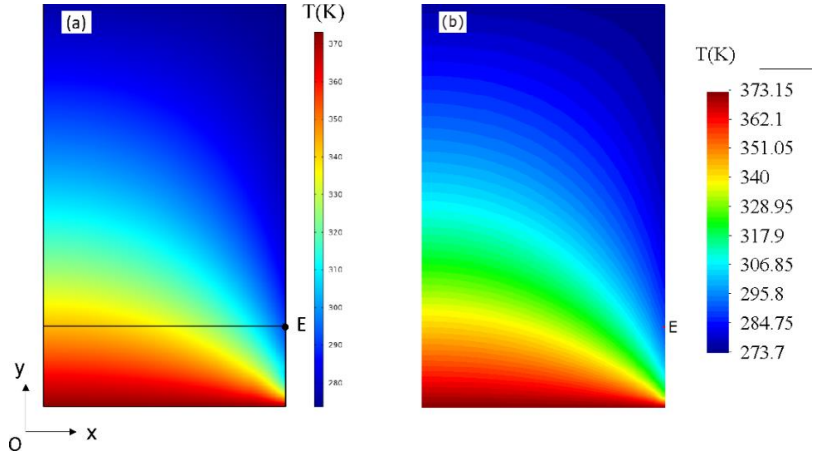

Figure 3. Temperature field obtained by Comsol (a) and Lagamine (b) for meshing case 4 with four integration points (IP = 4).

3. Thermal analysis of a DED process

3.1. DED of a bulk sample

The thermal histories experimentally recorded using thermocouples during a DED process of a bulk sample are the validation targets in our study, based on the experimental procedures and measurements detailed in references (Jardin et al., 2020; Jardin et al., 2019). Fig. 4 illustrates the DED process, the built sample, and the positions of four thermocouples attached to the substrate to measure the thermal evolution during the experiment. The sample was built by depositing 36 layers with 27 tracks using a horizontal back-and-forth line-scanning strategy. In addition, a substrate preheating temperature of 300°C was applied to reduce the cracking susceptibility encountered in the deposited component, especially in the case of the high-speed tool steel (Baek et al., 2017; Shim et al., 2017).

3.2. Thermal analysis using finite element method

In (Mertens et al., 2020; Jardin et al., 2019), a 2D FE model was developed to simulate the DED process of a bulk sample to reduce the computational time as compared to a full 3D model. Although the 2D FE model cannot provide information in the remaining direction, its predictions about the thermal history and melt pool depth provide helpful information for the process parameter determination before the experiment. The usefulness of the 2D FE models in DED simulation has been proved in the literature for different materials (Parekh et al., 2016; Ya et al., 2016). The assumptions of the 2D FE simulation for a 3D problem were discussed and detailed in Fetni et al. (2021). The FE simulations conducted in our study aimed to compare the performance between the two solvers Lagamine and Comsol, for the DED application.

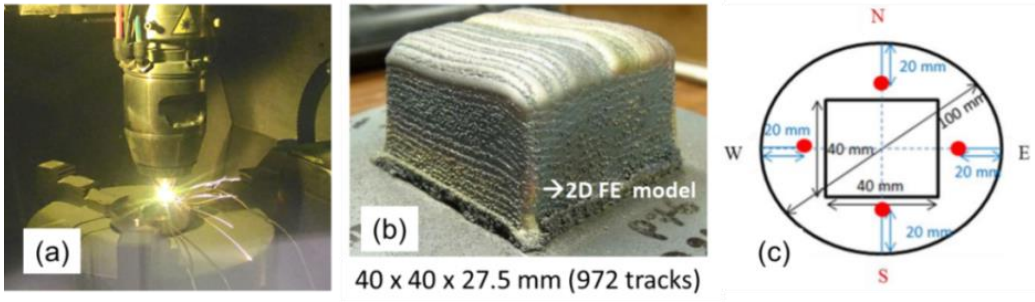

Figure 4. DED process (a), the built bulk sample (b), and the positions for the thermal measurement in the substrate by four thermocouples (c).

In this study, the model consists of a planar mesh simulating the vertical section in the middle of the whole geometry, including the deposit, substrate, and two blocks used as the sample holder; and parallel to the laser depositing direction, as shown in Fig. 5. The substrate and cladding regions were modeled using thermo-mechanical four-node quadrilateral elements BLZ2T defined in the Lagamine code (Hashemi, 2017). For this type of element, the numerical integration over the element domain can be performed

either with the first-order Gaussian integration method (IP = 1) or the second-order Gaussian integration method (IP = 4).

The Lagamine mesh was then transferred into the Comsol software through an input file (*.mphtxt). For this purpose, a Python script was developed to generate the Comsol input file from the Lagamine input file (*.lag). This script aims to convert all the BLZ2T elements of Lagamine to the "QUAD" elements in Comsol, in which the integration is numerically approximated using the second-order Gaussian integration method. The development of the script is straightforward and is not detailed in this study.

Fig. 5 shows the meshes used for both Lagamine and Comsol. In this model, a fine mesh of 0.75x0.764 mm2, corresponding to the element width and height, was applied to the deposit; whereas, the substrate and sample holder blocks were meshed by coarser elements. It should be noted that the element width of 0.75 mm corresponds to half of the laser spot size. The model contains 2,519 nodes with 2,426 elements. This study adopted the temperature-dependent material properties of the high-speed steel (M4 grade) powder and those of the substrate reported in Jardin et al. (2019).

The governing equation for 2D transient heat conduction is given using the following equation:

$$\frac{\partial}{\partial x}\left(k\frac{\partial T}{\partial x}\right)+\frac{\partial}{\partial y}\left(k\frac{\partial T}{\partial y}\right)+q_{int}=\rho C_p\frac{\partial T}{\partial t} \quad (2)$$

where T(x, y, t) denotes the transient temperature; k is the thermal conductivity; C_p is the specific heat capacity; ρ is the mass density; q_{int} denotes the internal energy generation per volume in the workpiece; t denotes the interaction time. In addition, the heat fluxes due to convection and radiation, which transfer the internal energy to the environment, are defined as follows:

$$q_{con}=h(T-T_0) \quad (3)$$

$$q_{rad}=\sigma\varepsilon(T^4-T_0^4) \quad (4)$$

where h is the convection coefficient; T_0 is the ambient temperature; σ is the Stefan-Boltzmann constant (5.67x10-8 W/(m2•K4)); and ε is the surface emissivity.

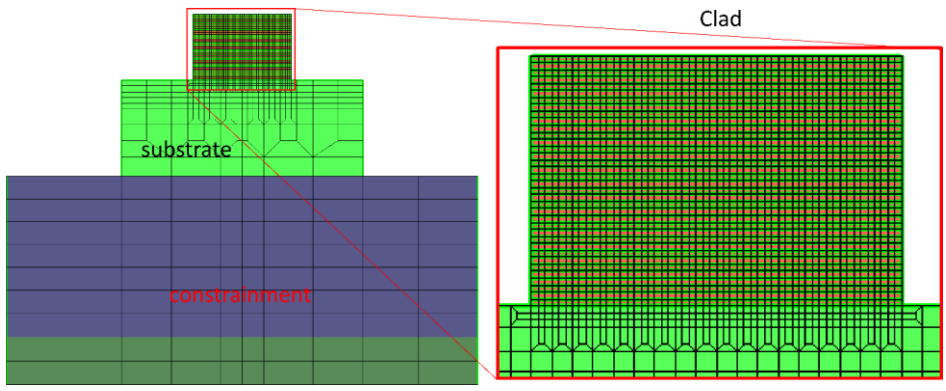

Figure 5. Full mesh for the 2D FE model.

3.3. Comparison between Lagamine and Comsol modeling approaches

There exist several approaches to model the DED thermal phenomena using FE simulations. The following subsections detail the differences between Lagamine and Comsol in numerical modeling approaches as well as solver configurations.

3.3.1. Element activation

In order to model the continuous addition of materials within successive layers in a DED process, the element birth and death technique was used. Precisely, in the Lagamine code, all activated and deactivated elements need to be predefined at each computing time through a switch function described in an input file (*.swi). At a configured time, the contribution of deactivated elements to the global stiffness matrix is eliminated. Therefore, the rank of the stiffness matrix is recomputed at the beginning of each time increment. This avoids solving ill-conditioned equations in FE simulations. As a result, the derived solution is close to the real process and generally stable. However, preparing the input file (*.swi) requires laborious skills, which is not simple for the new users.

In order to deal with the material deposition in welding and AM processes, the "Activation" functionality has been introduced in Comsol (Danielsson, 2018). Accordingly, the activation function scales down the material conductivity to a negligible value when the considered elements are inactivated. Their thermal conductivity is then restored to a normal value with a newly deposited material volume in which these elements are activated. The activation scale factor reduces but does not eliminate the contribution of the inactivated elements to the global stiffness matrix. Therefore, imposing a too-low value on the scale factor could lead to an ill-conditioned stiffness matrix. In this study, a default value of 10^{-5} was adopted for the activation scale factor in Comsol.

3.3.2. Heat source modeling

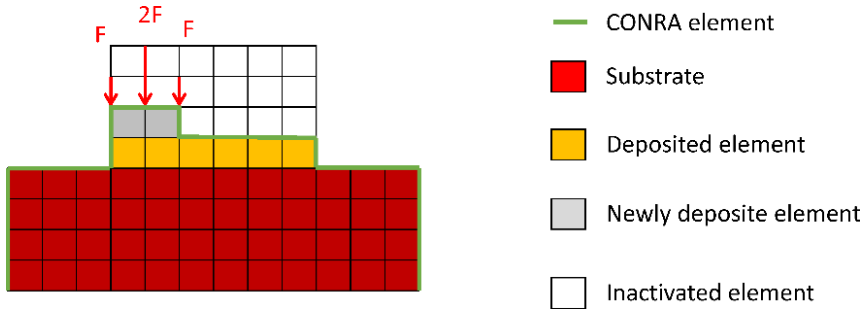

Figure 6. Representative image of the heat source modeling strategy and the CONRA element in the Lagamine code.

As mentioned in (Jardin et al., 2020; Jardin et al., 2019), a laser spot with a top-hat energy distribution was used to melt the material powders. The mean diameter of the laser spot is 1500 µm (1400 µm at the top and 1600 µm at the bottom), which corresponds to the width of two successive elements in the mesh design, as detailed in Section 3.2. In the numerical model of the Lagamine code, the external heat flux generated by the laser

source was modeled by concentrated heat fluxes acting on the top surface of three adjacent nodes of two newly activated elements, as shown in Fig. 6. In addition, the thermal powers applied on all surface nodes are listed in a Lagamine input file (*.loa) at every computational increment to describe the movement of the heat source.

In Comsol, the moving heat source is modeled using the "boundary heat source" function, which defines a heat flux embedded in the boundary (COMSOL, 2008). The position of the heat source center, defined as a function of the computational time, can be imported by several approaches: using variables, interpolation functions, or the path imported from CAD geometries. In this study, the interpolation function approach was adopted due to its relevance to the implementation of the Lagamine code. Consequently, a constant distributed heat flux acting on the boundary was employed, based on the distance from the considered point to the heat source center. The heat source parameters employed in the Comsol software are calculated simply to assure the equality of the total heat energies imposed in the two codes at any given instant.

3.3.3. Convection and radiation modeling

In the Lagamine code, two-node surface elements CONRA was used to describe the heat loss due to both convection and radiation. Convection and radiation are considered numerically occurring through the free surface of the deposit and the substrate. The convection and radiation coefficients in Lagamine simulations were adopted based on the calibration study reported in (Jardin et al., 2020; Jardin et al., 2019). Their values allow recovery of the temperature history measured at the substrate point N (see Section 3.4).

Comsol provides the surface-to-ambient radiation function to describe the radiation phenomenon (COMSOL, 2008). In this function, a conditional surface emissivity is defined using an "if" statement to switch on/off the radiation condition of the corresponding activated/inactivated elements. Convection can be taken into account in Comsol by applying an external heat source with a negative heat flux value. The magnitude of the heat flux is equal to the absolute value of the heat flux calculated from the convection equation (Eq. (3)) with the determined convection coefficient.

3.3.4. Solver configuration

Computing an FE analysis requires solving linear/nonlinear or time-dependent/independent systems of equations. As multiphysics commercial software, Comsol offers numerical solvers based on the type of problem to be solved (COMSOL, 2008). For example, for the heat transfer problem in the investigated DED process, Comsol suggests the first and second orders of Backward Differentiation Formula (BDF) solver for time-dependent equations, the direct method MUMPS (MUltifrontal Massively Parallel Solver) based on the LU decomposition for the linear system of equations, and the constant Newton method for nonlinear equations. In addition, professional users can easily select and modify the solver configurations in the Comsol software, depending on the requirements of their specific problems.

The solver configuration for the Lagamine code is fully controllable through the strategy input file (*ex.dat). Similar to the Comsol solver, the LU decomposition and the Newton method are used to solve linear and nonlinear equations, respectively. Furthermore, the Crank-Nicolson method, which is based on the trapezoidal rule and gives second-order convergence in time, is applied to solve time-dependent equations to speed up the computation (Crank & Nicolson, 1947).

A summary of the differences in modeling approaches and solver configurations between the Lagamine code and the Comsol software is presented in Table 2. It should be noted that the differences in the modeling approaches are unavoidable, whereas those in solver configurations can be adjustable based on the user experiences.

TABLE 2. Differences between the Lagamine code and the Comsol software in modeling approaches and solver configuration.

Differences		**Lagamine**	**Comsol**
Modeling approaches	Element activation	Activated/deactivated elements	Scale factor
	Heat source	Concentrated at the nodal level	Constant distribution at the layer level
	Convection	CONRA element at the element level	External heat flux at the layer level
	Radiation		Surface-to-ambient at the surface edge level
Solver configurations	Number of IP	1 or 4	4
	Time stepping method	Crank-Nicolson method	BDF method Order: 1-2
	Linear solver	LU decomposition	Direct method MUMPS based on the LU decomposition
	Nonlinear solver	Newton-Raphson	Constant (Newton) Damping factor of 0.9
	Criterion for convergence	Balance between the heat flux and temperature criteria with a norm of 0.001	Temperature norm of 0.01
	Max. number of iteration	14	5
	Acceleration	Not mentioned	Anderson acceleration

3.4. Comparison of computational results

To compare the solutions obtained by the Lagamine code and Comsol software, the temperature evolutions of six nodes, including five nodes of the cladding regions (P_1 to P_5) and one node of the substrate (N), were considered, as shown in Fig. 7. Node P_1 corresponds to the first element of the deposition. The other nodes P_2, P_3, P_4, and P_5, are located at the middle of layers 1, 5, 9, and 35, respectively. The temperature evolution of the substrate node was observed experimentally via the thermocouple attached at the relevant position during the fabrication.

3.4.1. Temperature evolutions at the observed points

To clarify the configuration of the two solvers, a sub-model was developed in both Lagamine code and Comsol software. The convection and radiation heat transfer processes, as well as the element activation techniques, were discarded in this sub-model. Additionally, the thermal analyses were set to terminate after the simulation time of 50 s (successful deposition of the 7th layer) to save computational time.

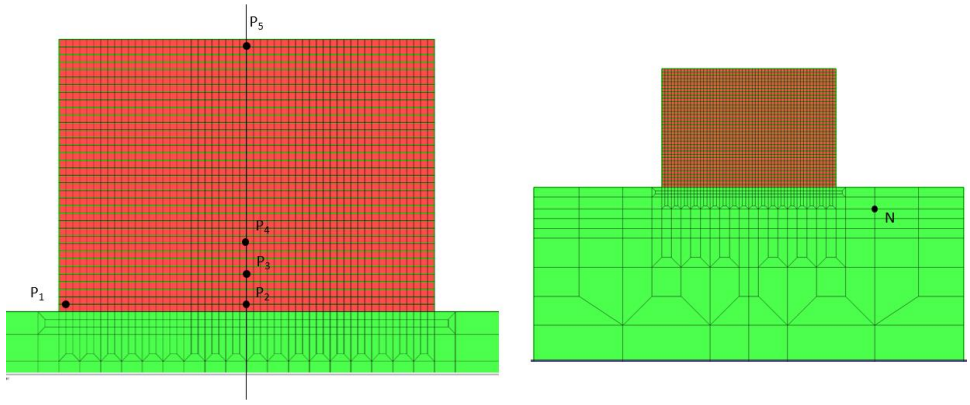

Figure 7. Locations of the observed points at which the temperature evolutions are compared between the Lagamine code and Comsol software.

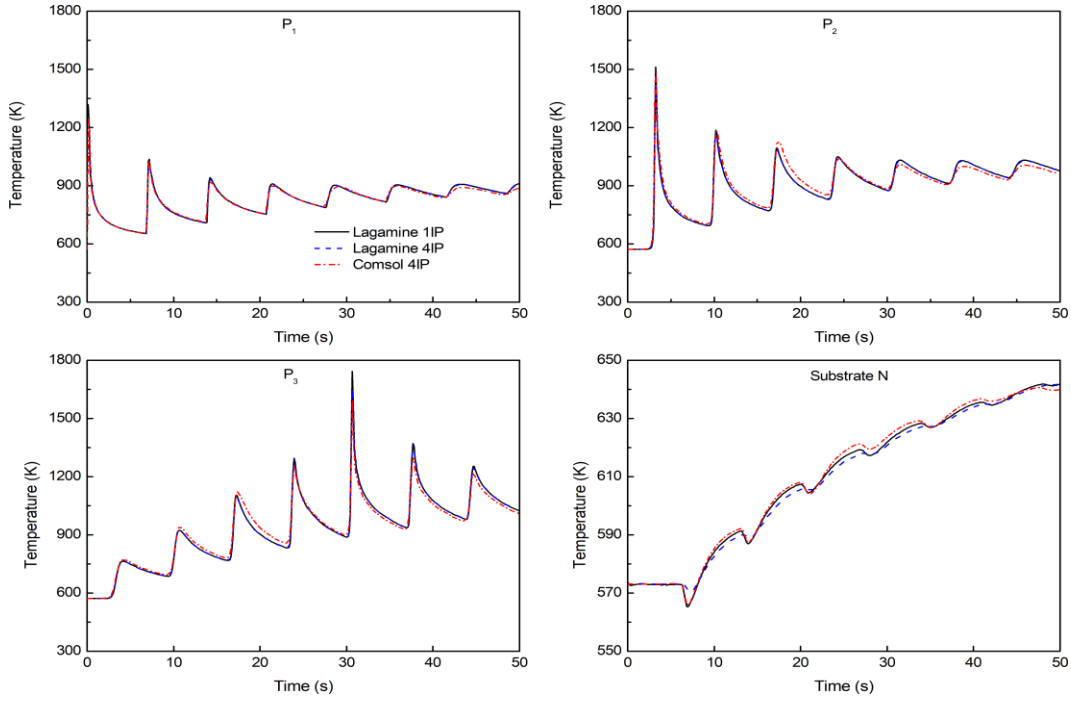

Figure 8. Temperature evolutions at several observed points are predicted by FE simulations without convection, radiation, and element activation.

Fig. 8 shows the temperature evolutions of five investigated points (P_1, P_2, P_3, and N) derived from these sub-models. Herein, the results obtained by the Lagamine code were calculated

with both one integration point (labeled by "Lagamine 1IP") and four integration-point (labeled by "Lagamine 4IP") methods; while the results of the Comsol software were obtained using only the four integration-point method (labeled by "Comsol 4IP").

As shown in Fig. 8, the temperature evolutions of all considered points predicted by the FE simulations using the Lagamine code are close to those derived from the Comsol software. Precisely, a slight difference of about a few tens of K in the highest peak temperatures was observed for three investigated points, i.e., P_1 and P_2 (see Fig. 8). However, the simulations using Lagamine 1IP and Lagamine 4IP provide a maximum difference in the highest peak temperature of about 100 K for point P_3, which is approximately equivalent to 7% of the Lagamine 1IP prediction. In the case of the four integration-point methods, Lagamine and Comsol predict the highest peak temperatures with a difference lower than 1%. Furthermore, it can be seen that the peak temperatures predicted by Lagamine 1IP are always higher than those derived from the simulations using Lagamine 4IP and Comsol. It is concluded that the internal element temperature gradient results in higher nodal values when the numerical integration less correctly describes the thermal field.

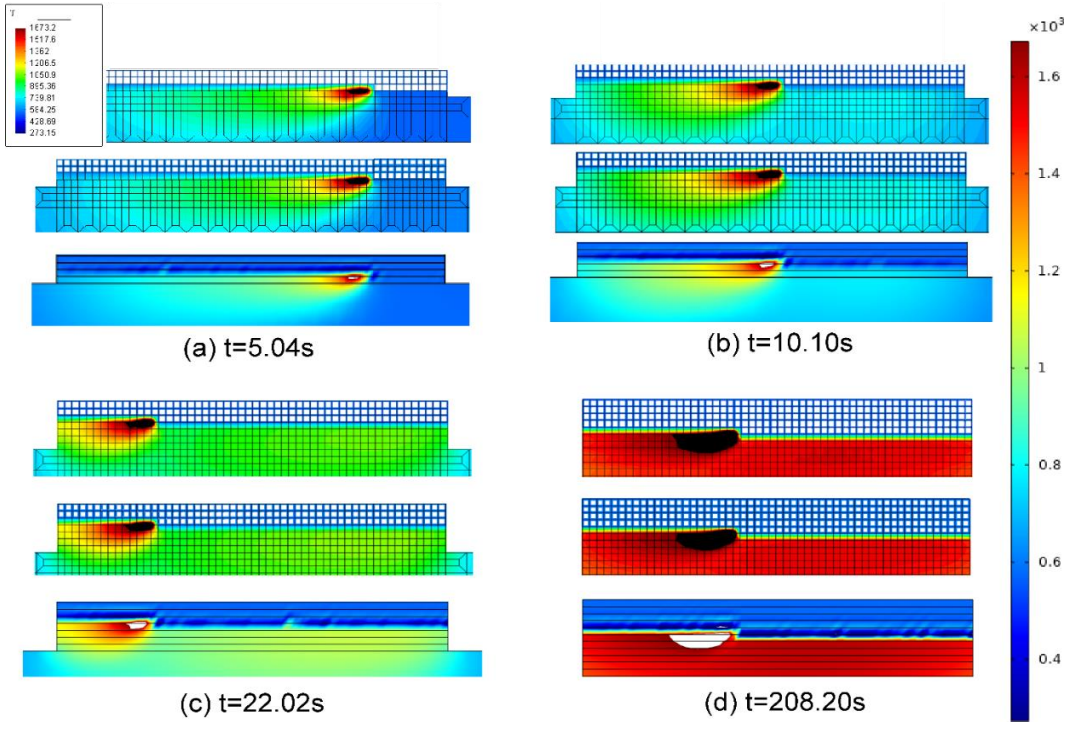

Figure 9. Comparison of the temperature distribution at different simulation times between Lagamine-1IP (top), Lagamine-4IP (middle), and Comsol (bottom). The black and white areas in the Lagamine and Comsol results correspond to predicted temperatures greater than the melting temperature of the studied material (1673.15 K).

To investigate the simulation accuracy of the DED process, a full FE model, including element activation, and heat losses resulting from convection and radiation, was

developed. Fig. 9 shows the thermal distribution within the whole model observed at different times using Lagamine and Comsol. In this figure, the black area of Lagamine results and the white area of Comsol results indicate the melting region. Imperfect solutions for inactivated elements near the last deposited layer were observed in the temperature field predicted by Comsol. The unexpected solutions could be explained by solving ill-conditioned equations generated by the element activation approach in Comsol. In contrast, the solutions of the Lagamine solver for the temperature field of these elements appear to be stable. Besides, the calculation domain of Lagamine is smaller than that of Comsol as the inactivated elements are not taken into account in the computation process of the Lagamine code. However, it should be noted that the stiffness matrix needs to be re-calculated by the Lagamine solver before each time increment.

Fig. 10 shows the temperature histories of substrate point N predicted by different solvers, as well as those experimentally measured by thermocouples during the fabrication. It can be seen that the measured curve exhibits various thermal cycles corresponding to the number of deposited layers. Within each cycle, several sub-peaks associated with printing tracks can be observed, as shown in Fig. 10 (b) with higher magnification. Since the temperature evolutions of different tracks cannot be modeled in a 2D model, the simulations conducted in our study focus on the prediction of the temperature evolution in the middle track. For this purpose, a numerical non-physic energy absorption coefficient was introduced in the Lagamine 1IP simulation to provide comparable predictions to the measurements. The value of this coefficient was calibrated in previous studies (Jardin et al., 2020; Jardin et al., 2019; Hashemi, 2017) and adopted in our work, leading to the values of the thermal input energy presented in Section 3.3.2. The same absorption coefficient, corresponding to the same thermal input energy, was applied to the other configurations, such as Lagamin 4IP and Comsol 4IP. However, the act yields deviated predictions of the temperature evolution of substrate point N, as shown in Fig. 10. Although the deviations are insignificant (e.g., always be less than 3%), they suppose the importance of parameter calibration with the selected FE code before simulation.

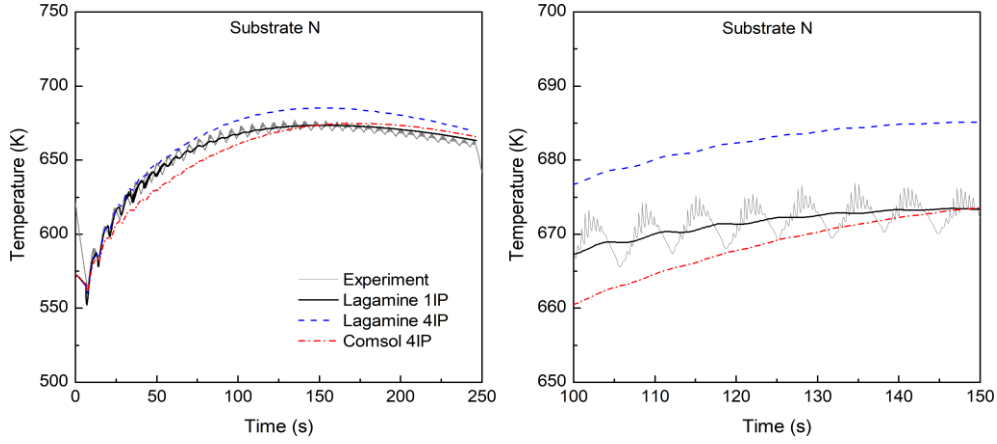

Figure 10. Temperature evolution at substrate point N is predicted by simulations with convection and radiation.

Fig. 11 shows the predictions of the temperature evolutions of five points located in the deposition regions. Generally, it is shown that the temperature predictions of the considered points based on two FE codes are similar for both peak temperatures and cooling periods. At each considered point, the temperature evolution increases, then decreases periodically according to the movement of the heat source. After several thermal loading cycles, for example, approximately 12 cycles for point P1 located in the first deposited layer, the thermal fluctuation can be considered as negligible. Subsequently, the temperature of this point decreases gradually. Within each thermal cycle, temperature histories predicted by different solvers for the cooling periods (e.g., the period shows negative temperature gradients) are close to each other. Therefore, the effect of FE solver selection on the prediction of cooling/solidification rates is estimated from these simulations.

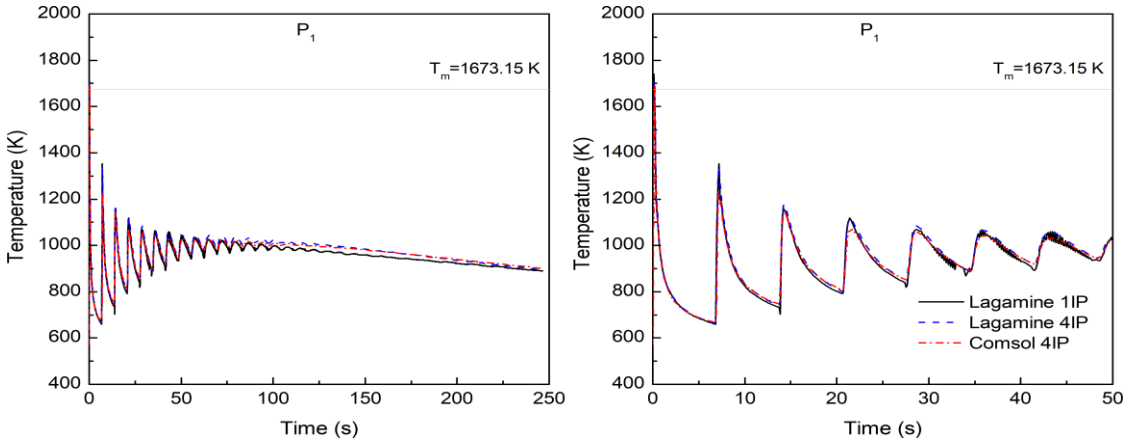

(a) P_1

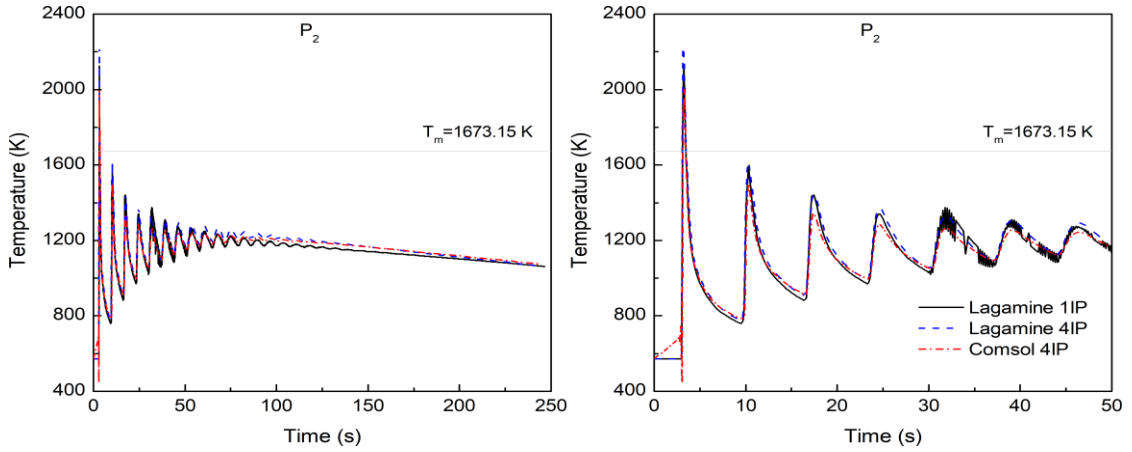

(b) P_2

Figure 11. Temperature evolutions at several considered points are predicted by simulations with convection, radiation, and element activation. The figures on the right are the magnified views of those on the left.

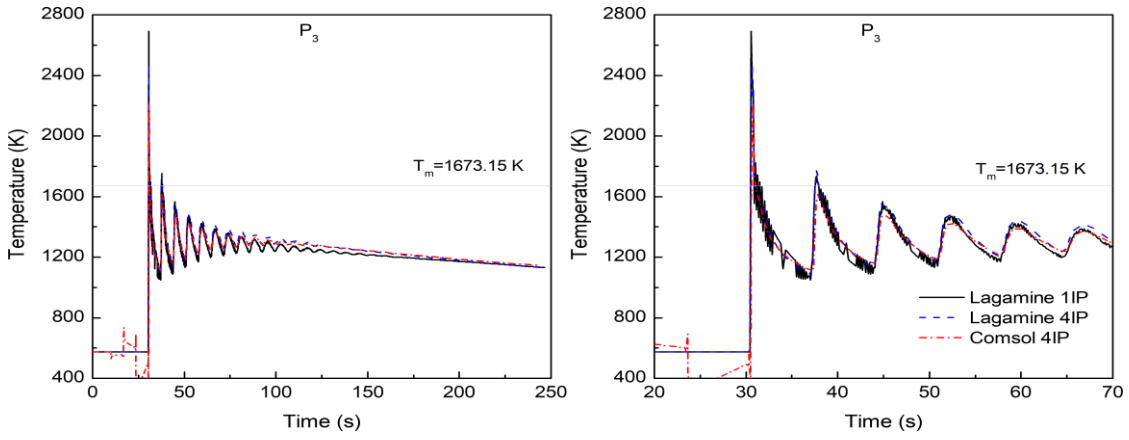

(c) P_3

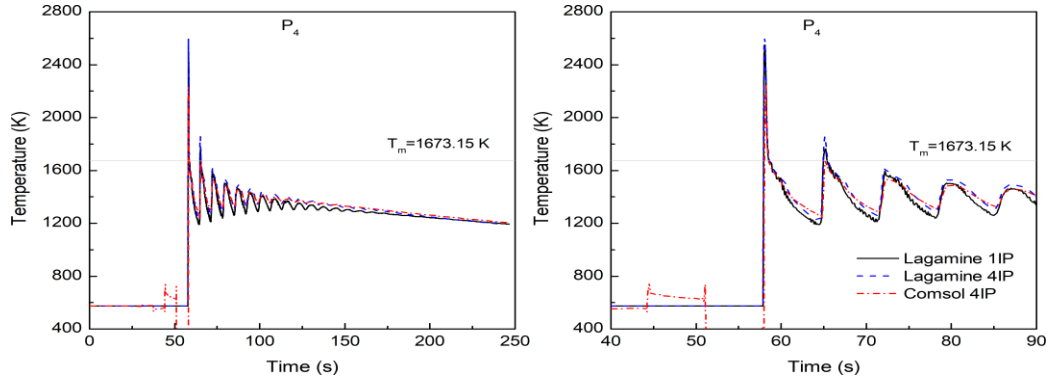

(d) P_4

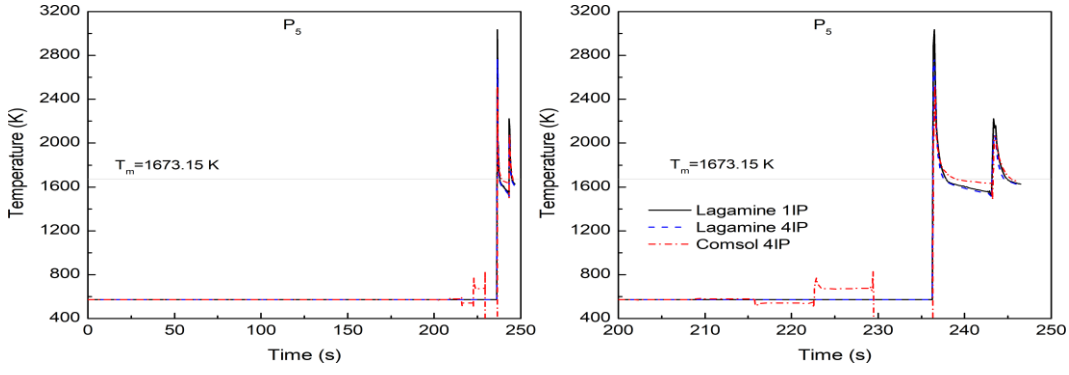

(e) P_5

Figure 11. Continued

In addition, Fig. 12 summarizes the highest peak temperature and the temperature recorded at the end of simulations for the investigated points in the deposition. Precisely, the differences in the temperatures at the end of the simulations of these points are negligible in both cases of the sub-models and full models. However, contrary results of the highest peak temperatures were observed in these figures. In detail, the differences between these predictions shown in Fig. 12a are almost unchanged through the considering points. In Fig. 12b, a difference of 3% is observed for point P1, which is

increased to 20% for point P5. Comparative results shown in Fig. 12 demonstrate the effects of modeling the convection, radiation, and element activations in these simulations.

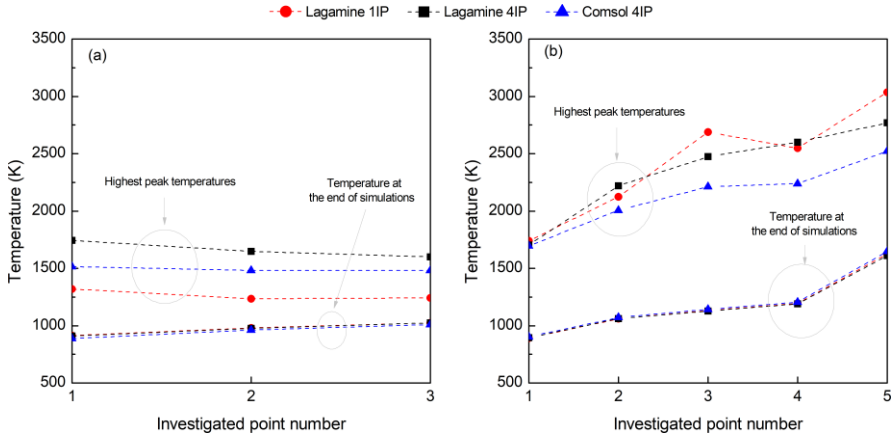

Figure 12. Prediction of the highest peak temperatures and temperatures at the end of simulations for considered points in the deposit (a) sub-models in Figure 8 and (b) full models in Figure 11.

Besides, the results shown in Fig. 11 and Fig. 12 indicate the effect of the element activation approaches used to describe the material deposition process. In the Lagamine switch approach, the contribution of the inactivated elements is eliminated. In contrast, the activation approach used in the Comsol software attempts to ignore but not eliminate the contribution of these inactivated elements. This explains the fluctuation of the temperature history predictions obtained by the simulation using the Comsol software for these considered points in the deposit before the activation of the corresponding elements characterized by the highest peak for each case (see Fig. 11). In contrast, the Lagamine code can predict a constant temperature corresponding to the initial temperature for all instants before the activations of these elements. This could result in lower highest peak temperatures predicted by the Comsol software as compared to those derived from the simulations performed by the Lagamine code, as shown in Fig. 12. Therefore, care should be taken when the predicted highest peak temperature is adopted in subsequent calculations, for example, in the solidification process during AM processes (Kumara et al., 2020; Tchuindjang et al., 2021; Xie et al., 2017).

3.4.2. Melt pool size

During a DED process, the size (and the morphology) of the melt pool potentially provides information on the fabrication quality as it strongly affects the microstructure and defect formation, e.g., lack of fusion or keyholing, within the deposit (Sampson et al., 2020). In an FE simulation, an element is considered to be melted if its temperature is higher than the melting temperature of the investigated material. Therefore, the melt pool size can be estimated numerically from the computed temperature field by

calculating the melted area of all activated elements. The maximum values of the melt pool size calculated from the FE predictions for each deposited layer are reported in Fig. 13. As can be seen in this figure, the Lagamine 4IP solver generates a nearly linear evolution of the melt pool size during the fabrication. In contrast, Lagamine 1IP and Comsol 4IP predict an exponential-like evolution of the melt pool size.

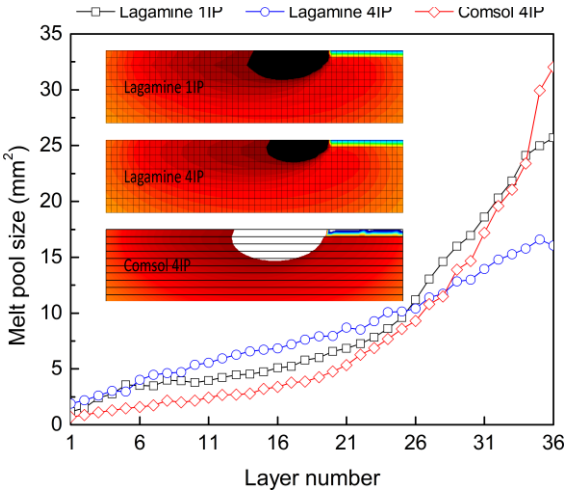

Figure 13. Comparison of the melt pool size estimated from the FE simulations conducted using different codes.

4. Discussion and conclusion

This study presents comparisons between the Lagamine and Comsol solvers for thermal analyses of a NAFEMS benchmark and a DED process of a bulk sample. In addition, technical issues in modeling the DED process based on the two codes are discussed. The following conclusions can be drawn from this work:

- In the NAFEMS benchmark, the Lagamine and Comsol solvers provide similar solutions that are nearly identical to the reference results in the case of the refined meshes and four integration point methods.
- For an especially assumed heat transfer problem in which convection and radiation are dismissed numerically, both Lagamine and Comsol provide similar results. However, for the DED simulation, which involves heat losses by convection and radiation as well as the element activation technique, two codes predict the highest peak temperatures with a significant difference. This may be explained by the differences in modeling approaches of the two codes, as highlighted in Section 3.3. Care should be taken to calibrate parameters related to the convection and radiation modeling of the selected FE code.
- As an in-house developed code, various Lagamine input files involve the numerical models of the moving heat source and boundary conditions encountered in DED processes. Therefore, training for new users in a general Lagamine simulation is more problematic than the Comsol software, which has been well-developed for generic

simulation problems. However, for a specific problem of the DED simulation, the use of the Lagamine code requires less effort than the Comsol due to the currently well-developed pre- and post-processing programs.

- Based on this study, both Lagamine code and Comsol software are consistent in performing more detailed investigations of the DED process, such as the influence of process parameters on the simulated results of the temperature fields.

Lagamine provides more flexible options to deal with numerical issues in developing an FE model to describe the DED process, such as element activation, convection and radiation heat transfer, and moving heat source modeling. Consequently, the development of a Lagamine model requires laborious skills, which are not easy for the new users. In contrast, the configuration in Comsol is a straightforward task with the support of the graphical user interface and various default options.

Acknowledgments

This research is funded by Thu Dau Mot University, Binh Duong Province, Viet Nam under grant number NNC.21.2.012.

References

A. Kiran, J. Hodek, J. Vavřík, M. Urbánek, J. Džugan (2020). Numerical simulation development and computational optimization for directed energy deposition additive manufacturing process, Materials (Basel). 13. https://doi.org/10.3390/ma13112666.

A. Mertens, J. Delahaye, O. Dedry, B. Vertruyen, J.T. Tchuindjang, A.M. Habraken (2020). Microstructure and properties of SLM AlSi10Mg: Understanding the influence of the local thermal history, *Procedia Manuf.* 47. 1089-1095. https://doi.org/10.1016/j.promfg.2020.04.121.

C. Kumara, A.R. Balachandramurthi, S. Goel, F. Hanning, J. Moverare (2020). Toward a better understanding of phase transformations in additive manufacturing of Alloy 718. *Materialia.* 13. https://doi.org/10.1016/j.mtla.2020.100862.

C.F. Guzmán, J. Gu, J. Duflou, H. Vanhove, P. Flores, A.M. Habraken (2012). Study of the geometrical inaccuracy on a SPIF two-slope pyramid by finite element simulations. *Int. J. Solids Struct.* 49. 3594–3604. https://doi.org/10.1016/j.ijsolstr.2012.07.016.

COMSOL (2008), Documentation for COMSOL Release 3.4, MA, USA.

D.G. Ahn (2021). Directed Energy Deposition (DED) Process: State of the Art. *Int. J. Precis. Eng. Manuf. - Green Technol*. 8. 703–742. https://doi.org/10.1007/s40684-020-00302-7.

D.S. Shim, G.Y. Baek, E.M. Lee (2017). Effect of substrate preheating by induction heater on direct energy deposition of AISI M4 powder. *Mater. Sci. Eng. A.* 682. 550–562. https://doi.org/10.1016/j.msea.2016.11.029.

Dassault Systèmes®, Abaqus Analysis User's Guide, (n.d.). https://www.3ds.com/products-services/simulia/services-support/support/documentation/.

E.L. Papazoglou, N.E. Karkalos, A.P. Markopoulos (2020). A comprehensive study on thermal modeling of SLM process under conduction mode using FEM. *Int. J. Adv. Manuf. Technol.* 111. 2939-2955. https://doi.org/10.1007/s00170-020-06294-7.

F. Pascon, S. Cescotto, A.M. Habraken (2006). A 2.5D finite element model for bending and straightening in continuous casting of steel slabs. *Int. J. Numer. Methods Eng.* 68. 125–149. https://doi.org/10.1002/nme.1715.

FEMLAB, FEMLab validation, (n.d.). http://femlab.narod.ru/heat.pdf (accessed August 13, 2021).

G.Y. Baek, K.Y. Lee, S.H. Park, D.S. Shim (2017). Effects of substrate preheating during direct energy deposition on microstructure, hardness, tensile strength, and notch toughness. *Met. Mater. Int.* 23. 1204–1215. https://doi.org/10.1007/s12540-017-7049-2.

H. Bikas, P. Stavropoulos, G. Chryssolouris (2016). Additive manufacturing methods and modeling approaches: A critical review. *Int. J. Adv. Manuf. Technol.* 83. 389–405. https://doi.org/10.1007/s00170-015-7576-2.

H. Tan, C. Zhang, W. Fan, F. Zhang, X. Lin, J. Chen, W. Huang (2020). Dynamic evolution of powder stream convergence with powder feeding durations in direct energy deposition, Int. *J. Mach. Tools Manuf.* 157. 103606. https://doi.org/10.1016/j.ijmachtools.2020.103606.

H.C. Tran, Y.L. Lo (2018). Heat transfer simulations of selective laser melting process based on volumetric heat source with powder size consideration. J. *Mater. Process. Technol.* 255. 411-425. https://doi.org/10.1016/j.jmatprotec.2017.12.024.

H.S. Tran, J.T. Tchuindjang, H. Paydas, A. Mertens, R.T. Jardin, L. Duchêne, R. Carrus, J. Lecomte-Beckers, A.M. Habraken (2017). 3D thermal finite element analysis of laser cladding processed Ti-6Al-4V part with microstructural correlations. *Mater. Des.* 128. 130–142. https://doi.org/10.1016/j.matdes.2017.04.092.

I. Neira Torres, G. Gilles, J. Tchoufang Tchuindjang, P. Flores, J. Lecomte-Beckers, A.M. Habraken (2017). FE modeling of the cooling and tempering steps of bimetallic rolling mill rolls. *Int. J. Mater.* Form. 10. 287–305. https://doi.org/10.1007/s12289-015-1277-0.

J. Crank, P. Nicolson (1947). A practical method for numerical evaluation of solutions of partial differential equations of the heat-conduction type. *Math. Proc. Cambridge Philos. Soc*. 43. 50–67. https://doi.org/10.1017/S0305004100023197.

J. Manie, G.-J. Schreppers, DIANA FEA User's manual, (n.d.).

J. Nie, C. Chen, L. Liu, X. Wang, R. Zhao, S. Shuai, J. Wang, Z. Ren (2021). Effect of substrate cooling on the epitaxial growth of Ni-based single-crystal superalloy fabricated by direct energy deposition, *J. Mater. Sci. Technol. 62*. 148–161. https://doi.org/10.1016/j.jmst.2020.05.041.

J. Pierry, X.C. Wang (1994). Finite element modelling of strain localisation in shear bands during a cutting process. *WIT Trans. Eng. Sci.* 6. 521–527. www.witpress.com.

J. Xie, V. Oancea, J.A. Hurtado (2017), Phase Transformations in Metals during Additive Manufacturing Processes, in: Nafems World Congr. https://www.researchgate.net/publication/319108651.

J.T. Tchuindjang, H. Paydas, H.-S. Tran, R. Carrus, L. Duchêne, A. Mertens, A.-M. Habraken (2021). A New Concept for Modeling Phase Transformations in Ti6Al4V Alloy Manufactured by Directed Energy Deposition. *Materials (Basel)*. 14. 2985. https://doi.org/10.3390/ma14112985.

K. Benarji, Y.R. Kumar, P. Ashwin (2020). Numerical simulation and experimental study on austenitic stainless steel by laser assisted metal deposition (L-MD). *Mater. Today Proc.* 39. 1497–1502. https://doi.org/10.1016/j.matpr.2020.05.460.

M. Courtois, M. Carin, P. Le Masson, S. Gaied, M. Balabane (2014). A complete model of keyhole and melt pool dynamics to analyze instabilities and collapse during laser welding. *J. Laser Appl.* 26. 042001. https://doi.org/10.2351/1.4886835.

M. Danielsson (2018). *How to Activate Material in Simulations of Manufacturing Processes, COMSOL Blog*. https://www.comsol.com/blogs/how-to-activate-material-in-simulations-of-manufacturing-processes/ (accessed July 26, 2021).

M.A. Chergui (2021). Simulation Based deposition Strategies Evaluation and Optimization in Wire Arc Additive Manufacturing. University Grenoble Alpes.

M.E. Stender, L.L. Beghini, J.D. Sugar, M.G. Veilleux, S.R. Subia, T.R. Smith, C.W.S. Marchi, A.A. Brown, D.J. Dagel (2018). A thermal-mechanical finite element workflow for directed energy deposition additive manufacturing process modeling. *Addit. Manuf. 21*. 556–566. https://doi.org/10.1016/j.addma.2018.04.012.

N. Hashemi (2017). Study of High Speed Steel deposits produced by Laser cladding Microstructure – Wear – Thermal model, University of Liege. https://orbi.uliege.be/handle/2268/214330.

N.S. Johnson, P.S. Vulimiri, A.C. To, X. Zhang, C.A. Brice, B.B. Kappes, A.P. Stebner (2020). Invited review: Machine learning for materials developments in metals additive manufacturing. *Addit. Manuf. 36*. https://doi.org/10.1016/j.addma.2020.101641.

NAFEMS (1990). *The Standard NAFEMS Benchmarks*. https://www.nafems.org/.

R. Parekh, R.K. Buddu, R.I. Patel (2016). Multiphysics Simulation of Laser Cladding Process to Study the Effect of Process Parameters on Clad Geometry. *Procedia Technol. 23*. 529–536. https://doi.org/10.1016/j.protcy.2016.03.059.

R. Sampson, R. Lancaster, M. Sutcliffe, D. Carswell, C. Hauser, J. Barras (2020). An improved methodology of melt pool monitoring of direct energy deposition processes. *Opt. Laser Technol.* 127. https://doi.org/10.1016/j.optlastec.2020.106194.

R.T. Jardin, J. Tchoufang Tchuindjang, L. Duchêne, H.S. Tran, N. Hashemi, R. Carrus, A. Mertens, A.M. Habraken (2019). Thermal histories and microstructures in Direct Energy Deposition of a High Speed Steel thick deposit. *Mater. Lett.* 236. 42–45. https://doi.org/10.1016/j.matlet.2018.09.157.

R.T. Jardin, V. Tuninetti, J.T. Tchuindjang, N. Hashemi, R. Carrus, A. Mertens, L. Duchêne, H.S. Tran, A.M. Habraken (2020). Sensitivity analysis in the modeling of a high-speed, steel, thin wall produced by directed energy deposition. Metals (Basel). 10. 1–24. https://doi.org/10.3390/met10111554.

S. Fetni, T.M. Enrici, T. Niccolini, H.S. Tran, O. Dedry, L. Duchêne, A. Mertens, A.M. Habraken (2021). Thermal model for the directed energy deposition of composite coatings of 316L stainless steel enriched with tungsten carbides. *Mater. Des.* 204. 109661. https://doi.org/10.1016/j.matdes.2021.109661.

T. DebRoy, T. Mukherjee, H.L. Wei, J.W. Elmer, J.O. Milewski, Metallurgy (2021). mechanistic models and machine learning in metal printing. *Nat. Rev. Mater.* 6. 48–68. https://doi.org/10.1038/s41578-020-00236-1.

T.N. Le, Y.L. Lo, H.C. Tran (2019). Multi-scale modeling of selective electron beam melting of Ti6Al4V titanium alloy. *Int. J. Adv. Manuf. Technol.* 105. 545–563. https://doi.org/10.1007/s00170-019-04188-x.

Tdyn, Two-dimensional thermal analysis, (n.d.). http://www.compassis.com/downloads/Manuals/Validation/Tdyn-ValTest7-Thermal_conductivity_in_a_solid.pdf.

U. Scipioni Bertoli, G. Guss, S. Wu, M.J. Matthews, J.M. Schoenung (2017). In-situ characterization of laser-powder interaction and cooling rates through high-speed imaging of powder bed fusion additive manufacturing. *Mater. Des. 135*. 385–396. https://doi.org/10.1016/j.matdes.2017.09.044.

W. Jiazhu, T. Liu, H. Chen, F. Li, H. Wei, Y. Zhang (2019). Simulation of laser attenuation and heat transport during direct metal deposition considering beam profile. *J. Mater. Process. Technol*. 270. 92–105. https://doi.org/10.1016/j.jmatprotec.2019.02.021.

W. Ya, B. Pathiraj, S. Liu (2016). 2D modelling of clad geometry and resulting thermal cycles during laser cladding. *J. Mater. Process. Technol.* 230. 217–232. https://doi.org/10.1016/j.jmatprotec.2015.11.012.

W.E. Frazier (2014). Metal additive manufacturing: A review. *J. Mater. Eng. Perform*. 23. 1917–1928. https://doi.org/10.1007/s11665-014-0958-z.

Y.Y. Zhu, S. Cescotto (1995). Unified and mixed formulation of the 4-node quadrilateral elements by assumed strain method: Application to thermomechanical problems. *Int. J. Numer. Methods Eng*. 38. 685–716. https://doi.org/10.1002/nme.1620380411.